

Sedapp v2021: a non-linear diffusion-based forward stratigraphic model for shallow marine environments

Jingzhe Li^{1,2}, Piyang Liu³, Shuyu Sun⁴(✉), Zhifeng Sun^{2,1}, Yongzhang Zhou⁵, Liang Gong⁶, Jinliang Zhang⁷, Dongxing Du^{1,2}

5

1. College of Electromechanics, Qingdao University of Science and Technology, Qingdao 266061, China
2. Geo-Energy Research Institute, Qingdao University of Science and Technology, Qingdao 266061, China
3. School of Science, Qingdao University of Technology, Qingdao, 266520, China
4. King Abdullah University of Science and Technology, Jeddah 23955-6900, Saudi Arabia
- 10 5. School of Earth Science and Geological Engineering, Sun Yat-sen University, Guangzhou 510275, China
6. School of New Energies, China University of Petroleum (EastChina), Qingdao 266555, China
7. Department of Geography, Beijing Normal University, Beijing 100875, China

Correspondence to: Shuyu Sun (frank.sun.sa@gmail.com)

Abstract

15 The formation of stratigraphy in shallow marine environments has long been an important topic within the geologic community. Although many advances have been made in the field of forward stratigraphic modelling (FSM), there are still some areas that can be improved in the existing models. In this work, the authors present our recent development and application of Sedapp: a new non-linear open-source R code for FSM. This code uses an integrated depth-distance related function as the 20 expression of the transport coefficient to underpin the FSM with more along-shore details. In addition to conventional parameters, a negative-feedback sediment supply rate and a differentiated deposition-erosion ratio were also introduced. All parameters were implemented in a non-linear manner. Sedapp is a 2DH tool that is also capable of running 1DH scenarios. Two simplified case studies were conducted. The results showed that Sedapp can not only assist in geologic interpretation, but is also an 25 efficient tool for internal architecture predictions.

Keywords: Forward stratigraphic modelling, continental shelf, R codes, fluvial-deltaic, continental fault basin

1 Introduction

Shallow marine areas are among the most active environments for sedimentation, where sea level, tectonism, climate all influence the interactions between land and sea. The sedimentary successions formed in these areas are an important record of the past interactions. In addition, shallow marine stratigraphic record itself can be an ideal hydrocarbon accumulation place. From this record, many theoretical and field studies have made great achievements and accumulated a wealth of data in the past decades.

In order to better interpret the specific processes and analyze internal architectures, many forward stratigraphic models (FSM) have been built for a range of temporal and spatial scales. These models can be roughly divided into two categories, according to their purposes. The first is a full source-to-sink type, which mainly analyzes the deposition and erosion processes from the perspective of the whole sediment chain. In addition to analyzing the depositional response in the downstream unloading area, this kind of model also deals with precipitation and tectonic uplift in the upstream catchments area, which directly determine water and sediment flux (Armitage et al., 2011; 2018; Ding et al., 2019; Guerit et al., 2019; Zhang J.Y. et al., 2020). The second, which we choose here, is a sink-dominant type, which focuses on analyzing the architectures and stacking patterns of the sedimentary results in a forward manner (Rivenaes, 1997; Dalman and Weltje, 2012; Granjeon, 2014; Li et al., 2020). This type generally does not consider how the sediments in the source area are entrained. Instead, it usually takes the sediment supply rate as a known condition. This kind of model is appropriate for rapid evaluation of the underground strata and prediction of potential hydrocarbon reservoirs by fitting some known evidences.

For long-term processes, sediment flux is usually assumed to be proportional to the topographic gradient. Thus, through the mass conservation law, a diffusion equation like Eq. (1) is generally used in FSM models (Paola, 2000).

$$\frac{\partial h}{\partial t} = \nabla \cdot (\Gamma \nabla h) \quad (1)$$

where h denotes the topography, t denotes the time and Γ denotes the transport coefficient. If Γ is a constant or it does not change with the unknowns, these models are usually called linear models.

55 Whereas if Γ changes with the primary unknown h , these models are called non-linear models.

In many cases, linear models are not very robust when the stratigraphic results and controlling factors are interactively connected. For example, topography evolution in the marine portion is seriously affected by the water depth, whereas water depth is generally a function of topography and sea level. In this case, non-linear models seem to be more suitable. Many existing non-linear models 60 define the transport coefficient using water depth-related functions (e.g., in Clarke et al .1983; Kaufman,1991; Syvitski and Hutton, 2001, the coefficient value was assumed to decrease exponentially with the water depth). Water depth models can work well in general coastal zones. However, in shallow marine environments with river injection, these models are not as effective, especially when reflecting the shoreline shape in plane view. Depositional processes around the river 65 mouth are more active than those at a distance, even when they are at the same water depth.

Additionally, according to Eq. (1), if Γ is fixed for a given site, deposition or erosion (i.e., $\partial h/t > 0$ or $\partial h/ \partial t < 0$) depend solely on the topographic gradient. However, in a basin, the efficiency of deposition and erosion can be very different, even if the slope, sediment supply, and water flux are the same. For example, some bed surface is “hardground”, which is very difficult to erode. While the 70 overlying deposition process is relatively easy. In this case, a distinction between the two processes seems necessary. For a long-term stratigraphic forming process, there may exist many sedimentary discontinuities, which may provide long enough time to generate a variety of "hardgrounds" (the missing time in the sedimentary record can be predominant according to Miall, 2015). Thus, we need to impose a ratio to differentially treat the efficiency of deposition and erosion besides the original diffusion process. Here we call it the efficiency ratio of deposition to erosion. While customizable 75 adjustment of this ratio is less involved in the existing FSM models. Although some source-to-sink models (e.g. Guerit et al., 2019) have introduced the distinction between deposition and erosion processes, the complex parameter settings still severely limit its practicability in a quick result-fitting. In addition, many existing models are not free or open-source, making it difficult for people to 80 reproduce and improve them.

In this paper, we propose a new non-linear FSM model, which is expected to add some new features to the existing models. This model is integrated into a framework called Sedapp, which is an

open-source and cross-platform application written in R. We use examples to show how this model works and test its effectiveness and convenience in reconstruction of sedimentary systems, revealing
85 their internal architectures.

2 Methodology

2.1 Mathematical model

The Sedapp mathematical model can be expressed as follows:

$$F_i \frac{\partial h}{\partial t} = \max \left(\nabla \cdot (\Gamma_i \nabla h), \frac{1}{Der} \nabla \cdot (\Gamma_i \nabla h) \right) + q \quad (2)$$

$$90 \quad \sum_i^n F_i = 1 \quad (3)$$

where F_i is the fraction of the i th class of sediment, h is elevation, t is time, ∇ is the nabla operator, Der is a user-defined parameter denoting the ratio of deposition to erosion (it can be a scalar, vector or tensor value depending on its temporal and spatial variability), Γ_i is the diffusion coefficient for the i th class of lithology, and q is the source term that is a function of coordinates and time (the source term is used only for endogenetic sedimentation, especially carbonates. If endogenetic sedimentation is ignored, the source term can be left out). Of these, h and F_i are the primary unknowns.

Note that Γ_i cannot be outside the parentheses because they are not constants but rather functions of spatial coordinates and time. The Γ can generally be expressed as:

$$\Gamma = \max(\alpha e^{-\frac{D(\mathbf{x}, h, sl)^\eta}{\beta}}, \alpha_{wd} e^{-\frac{Wd(\mathbf{x}, h, sl)^{\eta_{wd}}}{\beta_{wd}}}) + \varepsilon \quad (4)$$

100 where α/α_{wd} are preexponential factors (L^2/T), η/η_{wd} are distance indexes (no dimension), β/β_{wd} are spatial scale factors (L^η or $L^{\eta_{wd}}$), and ε is an adjustment factor (L^2/T) reflecting the environment energy. In particular, the distance function $D=D(\mathbf{x}, h, sl)$ and water depth function $Wd(\mathbf{x}, h, sl)$ change with spatial coordinates \mathbf{x} , topography h and the sea level sl , and they apply to the marine portion only.

When $Der = 1$ and $n = 2$, the 3D (actually 2DH, because h is another dimension perpendicular to x and y) scenario for Eq. (2) and Eq. (3) can also be expressed as:

$$F \frac{\partial h}{\partial t} = \frac{\partial}{\partial x} \left(\Gamma_1 \frac{\partial h}{\partial x} \right) + \frac{\partial}{\partial y} \left(\Gamma_1 \frac{\partial h}{\partial y} \right) + q(x, y, t) \quad (5)$$

$$(1 - F) \frac{\partial h}{\partial t} = \frac{\partial}{\partial x} \left(\Gamma_2 \frac{\partial h}{\partial x} \right) + \frac{\partial}{\partial y} \left(\Gamma_2 \frac{\partial h}{\partial y} \right) + q(x, y, t) \quad (6)$$

where x and y are spatial coordinates. This is especially suitable for cases dealing only with two classes of sediments for simplicity, where Γ_1 is the transport coefficient for sand and Γ_2 is the transport coefficient for mud.

For 2D (1DH) scenarios, especially along the section line through the river mouth, the distance related term is generally larger than the water depth related term, so the latter term within the max function in Eq. (4) is usually omitted. For convenience in coding, also ignoring the endogenetic sedimentation, Eq. (5), Eq. (6) and Eq. (4) can be simplified into:

$$F \frac{\partial h}{\partial t} = \frac{\partial}{\partial x} \left(\Gamma_1 \frac{\partial h}{\partial x} \right) \quad (7)$$

$$(1 - F) \frac{\partial h}{\partial t} = \frac{\partial}{\partial x} \left(\Gamma_2 \frac{\partial h}{\partial x} \right) \quad (8)$$

$$\Gamma_i = \alpha_i \cdot e^{-\frac{(c \cdot D(x, t))^2}{E}} + \varepsilon, i = 1, 2 \quad (9)$$

The joint effect of c and E in Eq. (9) is equivalent to that of β in Eq. (4). The variable c here, with a dimension of L^{-1} , is mainly used to facilitate the scale of distance and differentiate the transport characteristics of different sediment types (e.g., sand and mud). E is a denominator of an exponent. Its corresponding numerator is a transformed distance term, which could be regarded as a proxy to the river injection related hydraulic energy. In order to make the whole exponent dimensionless, the denominator and the numerator should have the same dimension. Thus, E could be considered as “hydraulic characteristic energy”. While for ε , it does not contribute very much to the deposition geometry around the shoreline. Instead, it could significantly affect the sedimentation deep in the basin. This seems to have little to do with the transportation capability originated from the river injection, instead the most appropriate description is as the energy inherent in the basin that carries the sediments to the basin centre.

2.2 Code Implementation

Sedapp was written in the R language and its solution was based on the finite volume method (FVM), which has the desired property of local mass conservation and has a clear physical meaning (Versteeg and Malalasekera, 2007; Moukalled et al., 2016; Liu P. et al., 2017). The cell-centered

variable arrangement method was used to store the unknowns at the grid element centroids. The non-linearity was implemented through stepwise iteration (Fig.1).

135 The brief work-flow within a single time step is as below:

- 1) Implement user-defined tectonic subsidence and update the topography;
- 2) Implement user-defined sea level and identify/update the shoreline location;
- 3) Solve the differential deposition/erosion function;
- 4) Implement the compaction and isostatic subsidence.

140 Step 3) is an important step. According to the hypothesis of diffusion-based FSM models, the change rate (by either deposition or erosion) is proportional to the gradient of the slope (Fernandes et al., 1997; Pelletier, 2013). If we use the diffusion equation/law directly without any differential treatments between deposition and erosion (in other words, Der is held at 1), it will be very difficult to treat some complex situations. For example, some bed surface is “hardground”, which is very difficult 145 to erode, whereas the overlying deposition process is relatively easy. Hence, for a given location, erosion and deposition could occur at different rates and Der may not be equal to 1. For example, if we wanted the erosion rate to be only 1/100 of the deposition rate, Der can be set to 100. Through the max() function in Eq. (2), for a deposition process (namely the $\frac{\partial h}{\partial t} > 0$), $\nabla \cdot (\Gamma_i \nabla h)$ would be larger than $\frac{1}{der} \nabla \cdot (\Gamma_i \nabla h)$, and $\nabla \cdot (\Gamma_i \nabla h)$ is used. Otherwise, the $\frac{1}{der} \nabla \cdot (\Gamma_i \nabla h)$ is used. If a non-erosion 150 case is desired, Der can be set to a very large value.

Generally, sediment supply rate cannot be directly defined through boundary condition settings since the latter can only determine the boundary slope. Therefore, Sedapp uses a negative-feedback strategy to define the sediment supply rate. At each time step, the total amount of deposition within a step is first calculated using the previously defined α_{test} , and then the adjusted α_{mod} is calculated by 155 Eq. (10):

$$\alpha_{mod} = \alpha_{test} \frac{V_{expected}}{V_{test}} \quad (10)$$

where α_{mod} denotes the modified α of this time step; $V_{expected}$ denotes the expected sediment increment, namely the sediment supply rate; and V_{test} denotes the computed sediment increment with α_{test} .

3 Characteristics

160 3.1 Nonlinear transport coefficients

The nonlinear transport coefficient is a feature of Sedapp. Sedapp's transport coefficient uses a function of both the distance from the estuary and the water depth. This feature makes it easier to simulate fluvial-deltaic processes in 2DH scenarios, which can reflect changes along the shore. Even in 1DH cases, this feature also has some advantages (see the discussion section for details).

165 Generally, a smaller c value in Eq. (9) results in a higher sediment travel distance and a larger distribution range when the total amount of sediment is fixed. For example, the c of mud is usually set to 50%-85% of sand, thus reflecting the differential deposition of sand and mud. In addition, the environment energy ε can also influence the sediment travel distance; e.g. a larger ε will make the sediment travel further. As sedimentation progresses, the position of the estuary may change, so the 170 distance from the estuary is updated at each time step to achieve the nonlinearity of Γ .

3.2 Differential and customizable deposition/erosion rate

175 During the actual deposition process, the properties of the underlying strata (such as compaction degree, lithology, and age, etc.), as well as some external environmental factors (such as temperature, humidity and pH value, etc.), will affect the erosion rate. Therefore, the customized treatment of erosion rate is another Sedapp characteristic.

In Sedapp, the deposition rate is a parameter that can be specified directly (for the adjustment process see section 2.2). Furthermore, the Der parameter is a user-defined parameter that controls the ratio of deposition rate to erosion rate. When Der is 1, the deposition rate is equal to the denudation rate (Fig.2a), and when Der value is 10 or 100, denudation is significantly weakened (Fig.2b). Theoretically, 180 if the value of Der is large enough, it is equivalent to completely eliminating the denudation effect. Der values should be customized according to the actual situation.

3.3 Customizable compaction

185 Compaction is an important geological process after sediment deposition, especially when the sediment thickness is very high. In Sedapp, the compaction process can be easily realized by setting the composition of lithology and porosity curves.

In this paper, we designed a pyramid-shaped mountain simulation commonly used by other

researchers (as shown in Fig.3, see Rivenaes, 1992 and Yuan et al., 2019 for reference). The Der value was set to 1. The sediment supply ratio of sand and mud was set to 1:1, and the porosity curve was set as shown in Fig.3d. After simulation, the top of the pyramid was denuded and the foot of the pyramid had deposited sediment of a given thickness.

To illustrate the effect of compaction, Sedapp introduces a scale factor that can enlarge the longitudinal scale. Fig.3a shows the original compression scale (that is, the scale factor was equal to 1), and the scale factors in Fig.3b and Fig.3c were 100 and 1000, respectively. It can be seen that sediment thickness at the foot of the pyramid in Fig.3c was significantly smaller than that in Fig.3a. The factors that caused these differences were not only depth but also the proportion of sand and mudstone and the shape of depth-porosity curves, which can be easily adapted to different scenarios by modifying the lithologic proportion and porosity-depth functions in Sedapp.

4 Verification of Sedapp

To identify how well the algorithm works within geological context, some simple benchmark simulations are given below.

4.1 Typical stacking patterns

Typical stacking patterns including forced regression, normal regression, and transgression can be formed (Fig.4) by fixing sediment supply while controlling the adjusted sea level rise rate.

During the period of sea-level decline, the shoreline moved seaward, and the onlap points also moved seaward and form the offlap and downlap stratigraphic termination structures (Fig.4a). During slow sea-level rise, the shoreline continued to move seaward, but the onlap points started to move landward, forming an onlap termination structure. At the other end, the downlap structure continued to exist. During rapid sea-level rise, the shoreline started to move landward and the onlap points also moved landward. At this time, downlap structure did not exist above the slope break, but may have existed below the slope break.

4.2 Typical two-cycle scenario

To demonstrate the complete base level changing process, this paper designed a simulation with two full sinusoidal cycles as shown in Fig.5. In the first cycle, the shoreline dropped and moved

seaward. Then it slowly rose and gradually moved landward until it reached the highest point and
215 tended to stabilize. The water depth of deposition in the strata gradually deepened from left to right on
the marine side (Fig.5a), and the sandy content reached a maximum around the shoreline (Fig.5b) near
the shoreline. In the strata on the land side, the sand content was stratified. The sand content was
relatively large during the early transgression and subsequently relatively small. The second cycle was
located above the first cycle and continued the same characteristics as the first cycle, but the deposition
220 range was enlarged and the average single layer thickness was thinner..

4.3 Case studies

1) Model 1

In order to better display the 2DH performance of Sedapp, this paper designed Model 1. Its
length and width ranges were both 200m, and the elevation range was about 10m. The mesh was $200 \times$
225 200 in x-y plane. The time span of the model was set at 10 Myr, and the step size was set at 0.5 Myr.
Sea level was kept constant at 3 m. The initial topography was set as shown in Fig.6a. A river was set
up in the central position of the y-axis ($y = 100$ m). The channel shape of the river was set in advance as
a sine curve. The fluvial profile slope was set to a constant of 0.00357, and the sediment supply rate
was not defined since it could vary according to the fluvial profile slope. The other main parameters of
230 the model are shown in Tab. 1.

Projection of the simulation results on the x-y plane clearly showed the variability along the
shore (Fig.7). When $t = 0$, the shoreline was a straight line, and the channel was in the middle of the
shoreline. As time went on, the river mouth continued to move forward. From 0 to 2 Myr, the channel
first swung to the north, then to the south, and the shoreline began to bulge slightly towards the sea side.
235 From 2Myr, the channel continued to swing southward, until the time approached 4Myr and the river
mouth began to slowly turn north. From 4Myr to 6Myr, the channel continued to swing northward, and
the convex part towards the sea side became more prominent. From 6Myr to 8Myr, the channel
continued the previous trend, while the convex shoreline became asymmetrical (increasing skewness to
the north). From 8 Myr to 10 Myr, the principal line of the channel moved southward, and the convex
240 shoreline gradually returned to being symmetrical (Fig.7).

The simulation results also revealed some interesting features in longitudinal sections (Fig.8).
Two sections ($y = 75$ m and $y = 125$ m) perpendicular to the shoreline direction were selected (see Fig.7f

for the position of the section line). The two sections are located on the north and south sides of the main channel. The distance between the channel and the two sections was variable. In the southern profile (y = 75m), from 4 Myr to 10 Myr, the isochronous lines of the formation changed from sparse to dense, and then from dense to sparse (i.e., the thickness of a single clinoform changed from thick to thin first and then from thin to thick) (Fig.8). This was completely contrary to what was observed in the northern profile (y = 125m). From 4Myr to 10Myr, the isochronous lines first changed from dense to sparse, and then from sparse to dense, reflecting that the deposition rate first increased and then decreased (Fig.9).

Under the parameters shown in Tab. 1, due to the existence of estuaries, the shoreline bulged towards the sea side. A closer distance to the river mouth would result in a higher sedimentation rate and a greater shoreline advancing speed. From 2 Myr, the convex shape of the shoreline towards the sea side became more apparent, similar to the morphology of some real-world deltas (Fig.10).

255 2) Model 2

This code can be applied not only to marginal marine environments but also to the continental fault basins. Taking the 3 + 4 sand groups of the third member of Shahejie Formation in the Gaobei slope belt of Nanpu Sag in Bohai Bay Basin as an example, we conducted a simplified 1DH real case study. The basic geological background is as follows: During the deposition period of this set of strata, 260 the normal fault tectonic movement in the north of the sag was active, which was the main controlling factor leading to the increase of accommodation space. At the same time, the terrigenous clasts came from the north is sufficient, and the basin was in a balanced state (Li et al., 2018). According to the geological background, a simplified reconstruction model (Model 2) was designed, which assumed that the subsidence rate of the boundary fault and sediment supply rate is constant, neglected the effect of 265 isostasy, and considered the effect of sediment compaction.

The simulation results are shown in Fig.11. From the perspective of temporal and spatial stratigraphy, the shoreline mainly moved towards the sag center during the early stage, and then moved back to the land side. The deepest water depth occurred in the middle south part at 2 Myr (Fig.11a). This shoreline phenomenon is usually called autoretrete (Muto and Steel, 2002). The sand fraction 270 section shows that the steep slope belt in the north was richer in sand content than the south (Fig.11b). The porosity section shows that porosity generally decreased from bottom to top. The porosity also varied horizontally, especially when the depth was greater than 800 m. The porosity in the north was

higher than in the south.

275 Due to the over-simplified assumptions, the simulation results would not necessarily be consistent with every practical borehole. However, the simulation revealed general trends that can strengthen or improve our existing understanding and validate the previously proposed conceptual model.

5 Discussion

280 Sedapp is a diffusion-based model and its transport coefficient is a function of both distance from estuary and water depth. Compared with most existing diffusion models based only on water depth, this modification has great advantages in fluvial-deltaic environments, especially for 2DH scenarios. Sedapp not only simulates some surface landscapes, but it also reveals some interesting internal features. In the sections beside the channel in Model 1, the formation rate of the clinoforms had a close relationship with distance between the channel and the section. This may be of great significance for 285 analyzing ancient strata. Considering the resolution of seismic data, it is easier to observe changes in the density of the foreset than to directly find a channel. This may provide some important supplementary information in areas with less borehole data. Sedapp also showed strong simulation ability in 1DH scenarios. It can avoid some potential problems that water depth models may not overcome. For example, when the slope is steep, the slope break trajectory created by the water depth 290 model can even become far above the shoreline (Fig.12a and c). In contrast, Sedapp does not face such a problem. As long as the sea level is constant, the slope break line will remain in a straight line and the clinoforms will also move smoothly to the ocean (Fig.12b and d).

295 Sedapp can be used not only in shallow marine environment, but also in continental fault basins (Fig.11). In the case of Model 2 of Part 4.3, the simulation results of this study were very similar to those of the previous study (Li et al., 2018). In Li et al., 2018, the results were generated by Sedpak, an FSM model widely used in continental fault basins. Both Sedapp and Sedpak performed well in this case, while their core algorithms are different. Compared with the diffusion-based Sedapp, Sedpak is mainly geometry-based. Various geometric rules (e.g., alluvial angles, submarine angles, bypass angles, etc.) govern the processes in Sedpak. To generate a simple clinoform, setting a transport coefficient is 300 apparently more convenient than designing the above angles. This is an advantage of Sedapp over

Sedpak for beginner users. Another advantage of Sedapp over Sedpak is its flexibility in graphing. For example, the relative content of sand can only be expressed by discrete yellow and green belts in Sedpak. While in Sedapp, it is more flexible. A continuous colour bar is available, and the sand fraction can be expressed in a variety of ways due to its open-source feature.

305 The transport coefficient is a relatively long-term geomorphologic physical quantity, while wave, tidal, and current energy are relatively short-term hydrodynamic quantities. However, they are closely related. A river entering the sea is a type of jet flow phenomenon. The flow velocity decreases rapidly from the river mouth to the sea, which also has a strong negative correlation with the distance to the mouth of the river. The contour map of water flow velocity is fan-shaped. At the same time, the 310 decrease of velocity is also an important cause of sediment deposition, which also explains the close fan-shaped morphology of a delta front. Correspondingly, an increase in water depth will also decrease the flow velocity. For the open coast without river injection, a model based on water depth seems to be reasonable. However, for a coast with river injection, it is difficult to explain the formation of the 315 fan-shaped morphology of a delta. Therefore, it can be concluded that, in more general cases, the transport coefficient should be a function of short-term water energy, which is related to both the estuary distance and the water depth. When there is river injection, the river process is dominant and the estuary distance function is a reasonable proxy for the transport coefficient. When there is no river injection, the water depth plays the main role. In addition, particle size is also a decisive factor (Nash 1980; Andrews and Bucknam 1987). Hence, a choice function (see Eq. (9)) and differentiated α 's are 320 used to adapt different environments and lithologies. Although the current results of Sedapp seem plausible, these settings for transport coefficient are still empirical. Due to the complex nature of the transformation from short-term processes to long-term ones, it is difficult to build an accurate bridge between sediment hydrodynamics and stratigraphic formation, which may be the focus of the next step.

6 Code availability

325 The current version of model is available from the project website: <http://zenodo.org/record/4556868> or https://github.com/lijingzheQD/Sedapp_v2021 under the Creative Commons Attribution 4.0 International License. The exact version of the model used to produce the results used in this paper is archived on Zenodo. Input data and scripts of the case studies are also

presented in this site. For more details about Sedapp, please contact Jingzhe Li via email

330 lijingzhe@qust.edu.cn .

Contribution of each author

JL developed the main algorithm of Sedapp and took the lead in writing the manuscript. PL developed the FVM solver for Sedapp. PL, SS, ZS, YZ, LG, JZ and DD participated in the conceiving of the presented idea. SS supervised the project.

335 **Competing interests**

No conflict of interest exists in this manuscript.

Acknowledgement

Financial support was provided by the National Natural Science Foundation of China (42002169), the Initial Fund for Young Scholars of Qingdao University of Science and Technology, and the 340 Research Funding from King Abdullah University of Science and Technology (KAUST) through the grants BAS/1/1351-01. Jingfa Li from Beijing Institute of Petrochemical Technology, Jie Chen from Xi'an Jiaotong University and Hua Zhong from Guangdong University of Finance and Economics offered constructive advice in conceiving the model. We would like to thank Paul Halloran, John Armitage, Alberto Machado Cruz and an anonymous referee for their comments that greatly improved 345 our article. We would also like to thank the GMD editors for their careful and helpful editing work.

Reference

Andrews DJ, Bucknam RC. Fitting degradation of shoreline scarps by a nonlinear diffusion model. *Journal of Geophysical Research: Solid Earth*. 1987 Nov 10;92(B12):12857-67.

350 Armitage, J. J., Duller, R. A., Whittaker, A. C., & Allen, P. A. (2011). Transformation of tectonic and climatic signals from source to sedimentary archive. *Nature Geoscience*, 4(4), 231-235.

Armitage, J. J., Whittaker, A. C., Zakari, M., & Campforts, B. (2018). Numerical modelling of landscape and sediment flux response to precipitation rate change. *Earth Surface Dynamics*, 6(1), 77-99.

355 Athy, Lawrence Ferdinand. "Density, porosity, and compaction of sedimentary rocks." *Aapg Bulletin* 14, no. 1 (1930): 1-24.

Dalman RA, Weltje GJ. SimClast: An aggregated forward stratigraphic model of continental shelves. *Computers & geosciences*. 2012 Jan 1;38(1):115-26.

360 Ding X, Salles T, Flament N, et al. Quantitative stratigraphic analysis in a source-to-sink numerical framework. *Geoscientific Model Development*, 2019, 12(6).

Fernandes, Nelson F., and William E. Dietrich. "Hillslope evolution by diffusive processes: The timescale for equilibrium adjustments." *Water Resources Research* 33, no. 6 (1997): 1307-1318.

365 Granjeon, D. 3D forward modelling of the impact of sediment transport and base level cycles on continental margins and incised valleys. *From Depositional Systems to Sedimentary Successions on the Norwegian Continental Margin* (2014): 453-472.

Guerit, L., Yuan, X. P., Carretier, S., Bonnet, S., Rohais, S., Braun, J., & Rouby, D. (2019). Fluvial landscape evolution controlled by the sediment deposition coefficient: Estimation from experimental and natural landscapes. *Geology*, 47(9), 853-856.

370 Kaufman P, Grotzinger JP, McCormick DS, Franseen EK, Watney WL. Depth-dependent diffusion algorithm for simulation of sedimentation in shallow marine depositional systems. In *Sedimentary Modeling: Computer Simulations and Methods for Improved Parameter Definition 1991* (Vol. 233, pp. 489-508). Kansas Geological Survey Bulletin.

Li J, Liu P, Zhang J, Sun S, Sun Z, Du D, Zhang M. Base Level Changes based on Basin Filling Modelling: a Case Study from the Paleocene Lishui Sag, East China Sea Basin. *Petroleum Science*, 2020, 17 (5). <https://doi.org/10.1007/s12182-020-00478-2>

375 Li J, Zhang J, Sun S, Zhang K, Du D, Sun Z, Wang Y, Liu L, Wang G. Sedimentology and mechanism of a lacustrine syn-rift fan delta system: A case study of the Paleogene Gaobei Slope Belt, Bohai Bay Basin, China. *Marine and Petroleum Geology*. 2018 Dec 1;98:477-90.

Liu P, Yao J, Couples G D, et al. Numerical modelling and analysis of reactive flow and wormhole formation in fractured carbonate rocks. *Chemical Engineering Science*, 2017, 172: 143-157.

380 Miall, A. D. (2016). Stratigraphy: the modern synthesis. In *Stratigraphy: A modern synthesis* (pp. 382-386). Springer, Cham.

Moukalled F, Mangani L, Darwish M. The finite volume method in computational fluid dynamics. Berlin, Germany:: Springer; 2016.

385 Muto T, Steel RJ. Role of autoretreath and A/S changes in the understanding of deltaic shoreline trajectory: a semi - quantitative approach. *Basin Research*. 2002 Sep 1;14(3):303-18.

Nash DB. Morphologic dating of degraded normal fault scarps. *The Journal of Geology*. 1980 May 1;88(3):353-60.

390 Paola C. Quantitative models of sedimentary basin filling. *Sedimentology*. 2000 Feb;47:121-78.

Pelletier, Jon. "Fundamental Principles and Techniques of Landscape Evolution Modeling." In

Treatise on Geomorphology, pp. 29-43. Elsevier Inc., 2013.

Rivenaes JC. Application of a dual - lithology, depth - dependent diffusion equation in stratigraphic simulation. *Basin Research*. 1992 Jun 1;4(2):133-46.

395 Rivenaes JC. Impact of sediment transport efficiency on large - scale sequence architecture: results from stratigraphic computer simulation. *Basin Research*. 1997 Jun;9(2):91-105.

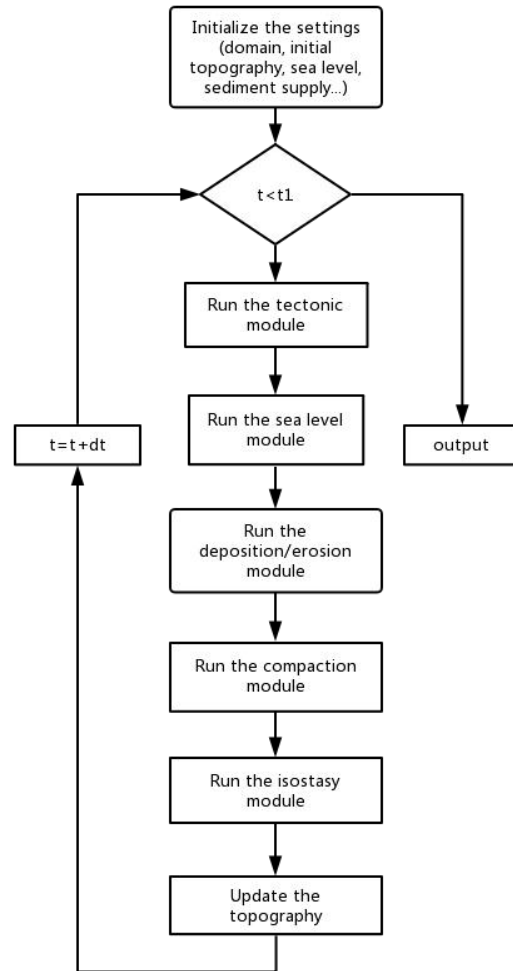
Sclater JG, Christie PA. Continental stretching: An explanation of the post - mid - Cretaceous subsidence of the central North Sea basin. *Journal of Geophysical Research: Solid Earth*. 1980 Jul 10;85(B7):3711-39.

400 Syvitski JP, Hutton EW. 2d sedflux 1.0 c:: an advanced process-response numerical model for the fill of marine sedimentary basins. *Computers & Geosciences*. 2001 Jul 1;27(6):731-53.

Versteeg HK, Malalasekera W. An introduction to computational fluid dynamics: the finite volume method. Pearson education; 2007.

405 Yuan XP, Braun J, Guerit L, Simon B, Bovy B, Rouby D, Robin C, Jiao R. Linking continental erosion to marine sediment transport and deposition: A new implicit and O (N) method for inverse analysis. *Earth and Planetary Science Letters*. 2019 Oct 15;524:115728.

Zhang J, Sylvester Z, Covault J. How do basin margins record long-term tectonic and climatic changes?[J]. *Geology*, 2020.



410

Fig. 1 Flowchart of the algorithms in Sedapp

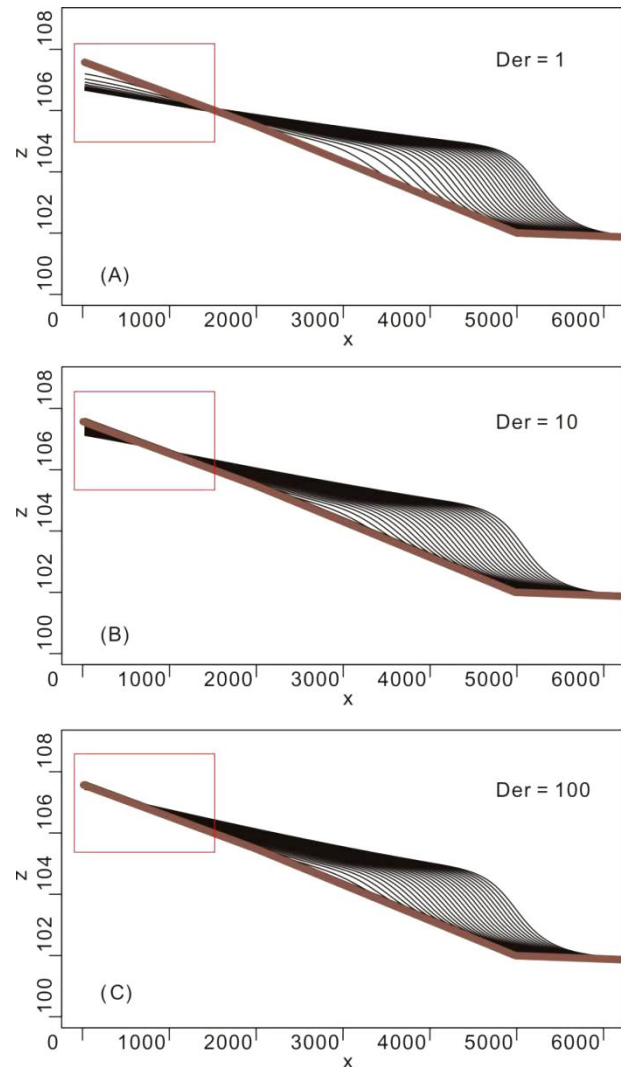
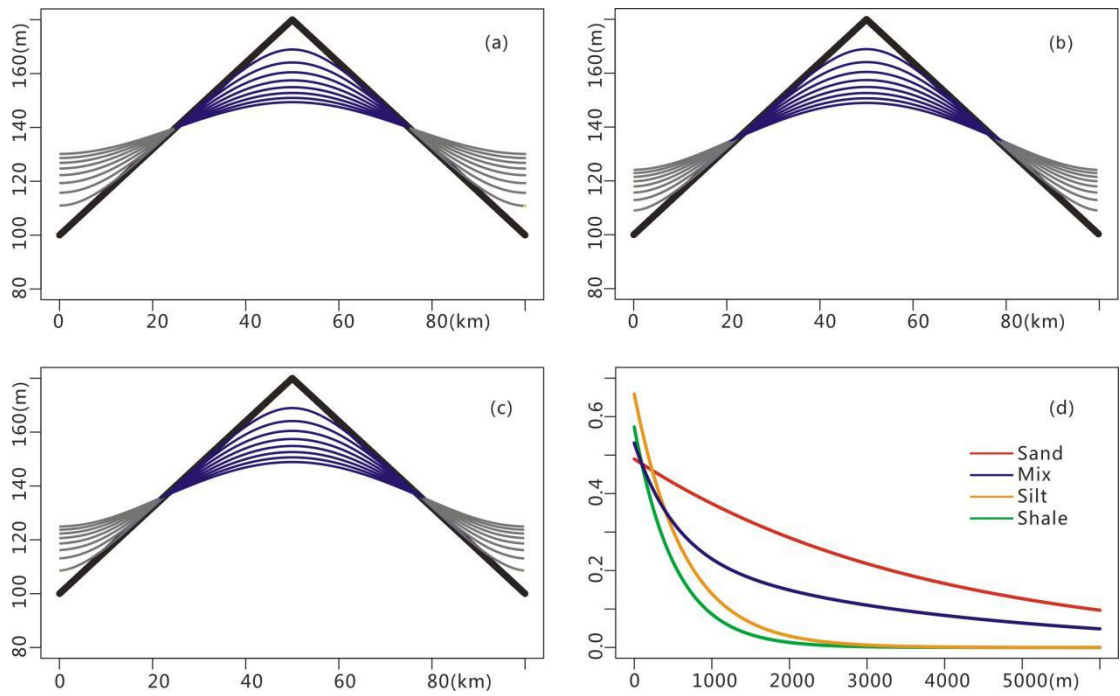


Fig. 2 Dip direction section with different Der values (Der = 1, Der = 10, Der = 100 respectively).

Erosion will be switched off if Der is large enough.



415

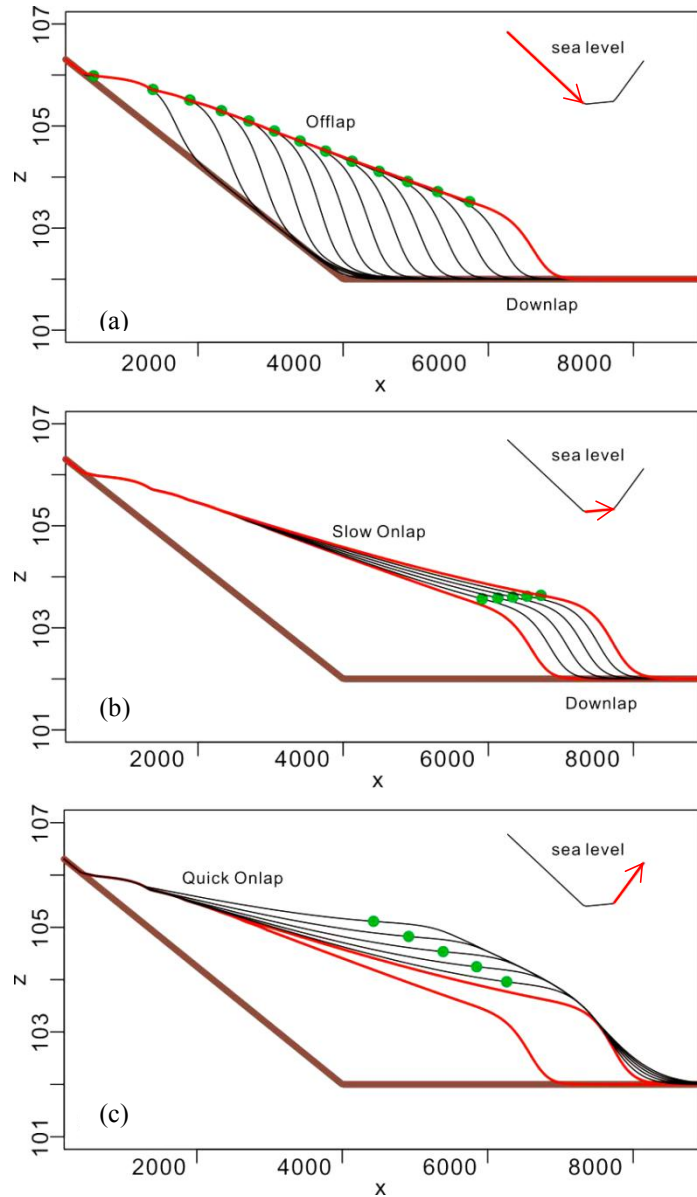
Fig. 3 Customized compaction and the porosity curves. a) the x-z plot with original

depth-porosity scale; b) the x-z plot with magnified depth-porosity scale (x100) to enhance compaction;

c) the x-z plot with magnified depth-porosity scale (x1000) to enhance compaction; d) Depth-porosity

curves used in the compaction module (the mix indicates mixed 50%-50% sand and shale. Details see

Athy, 1930; Sclater and Christie 1980)



420

Fig. 4 Typical stacking patterns acquired through different sea level change rates

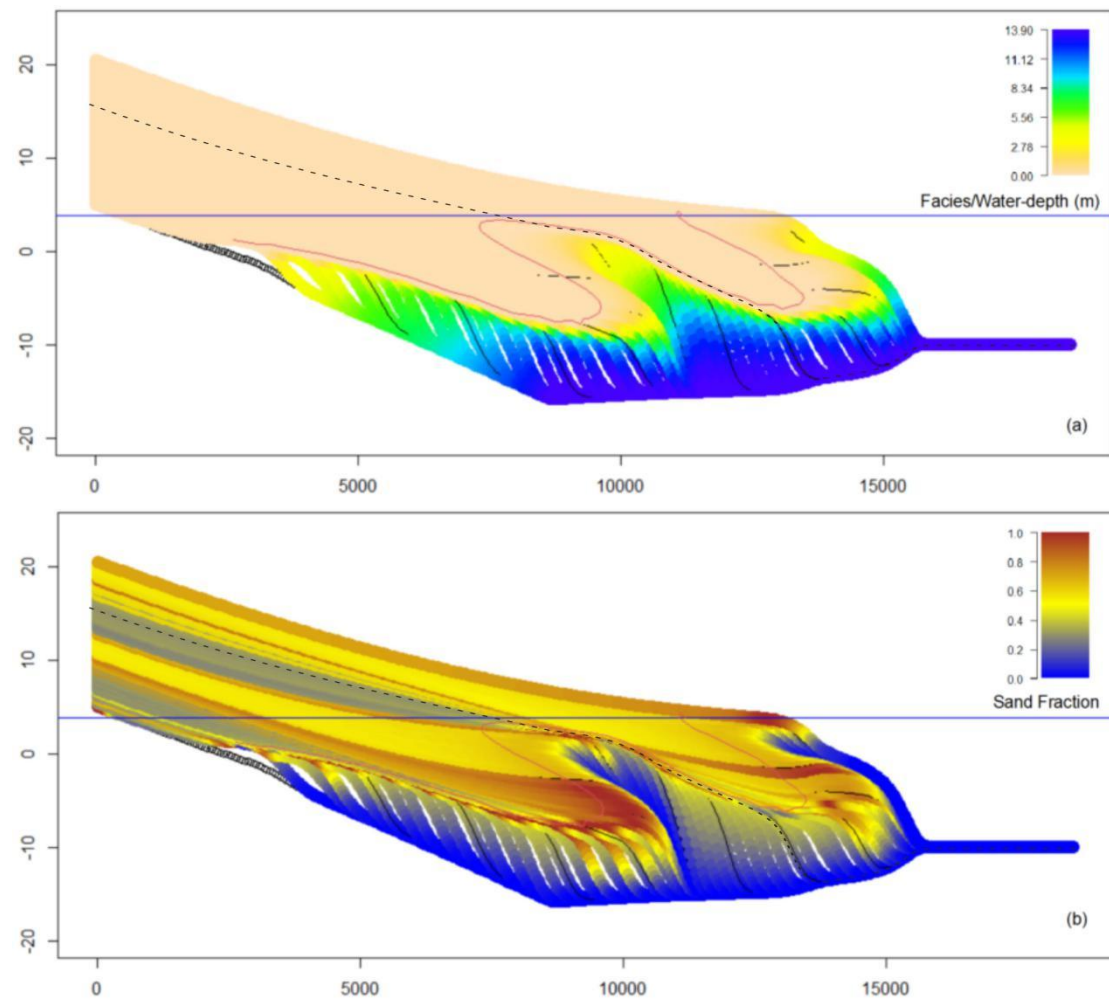


Fig. 5 Simulated stratigraphy under two full sea level cycles. A) facies section and B) lithological section.

425

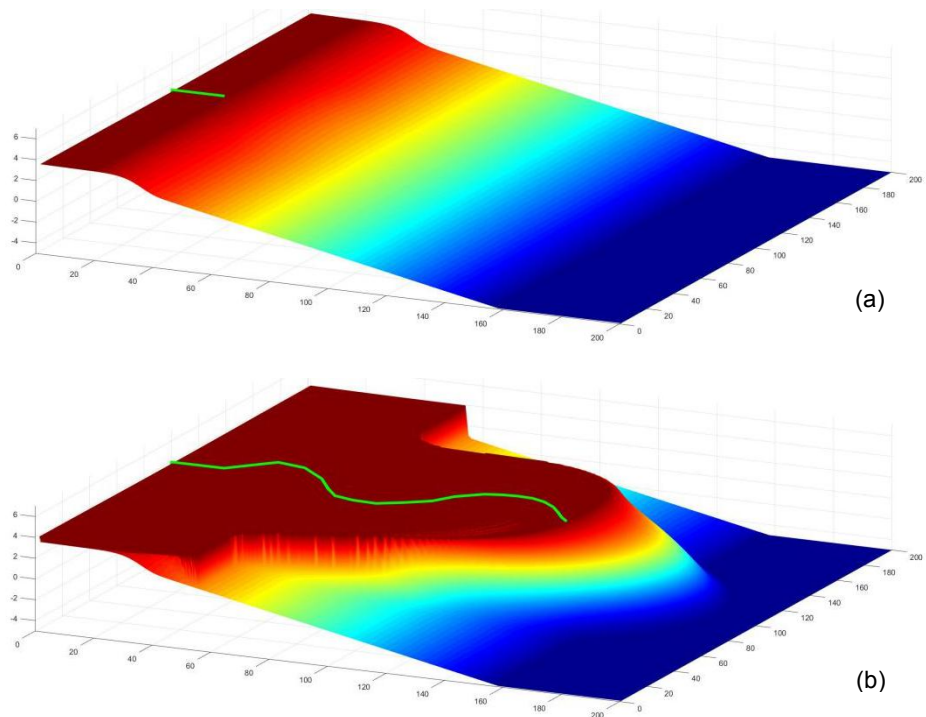
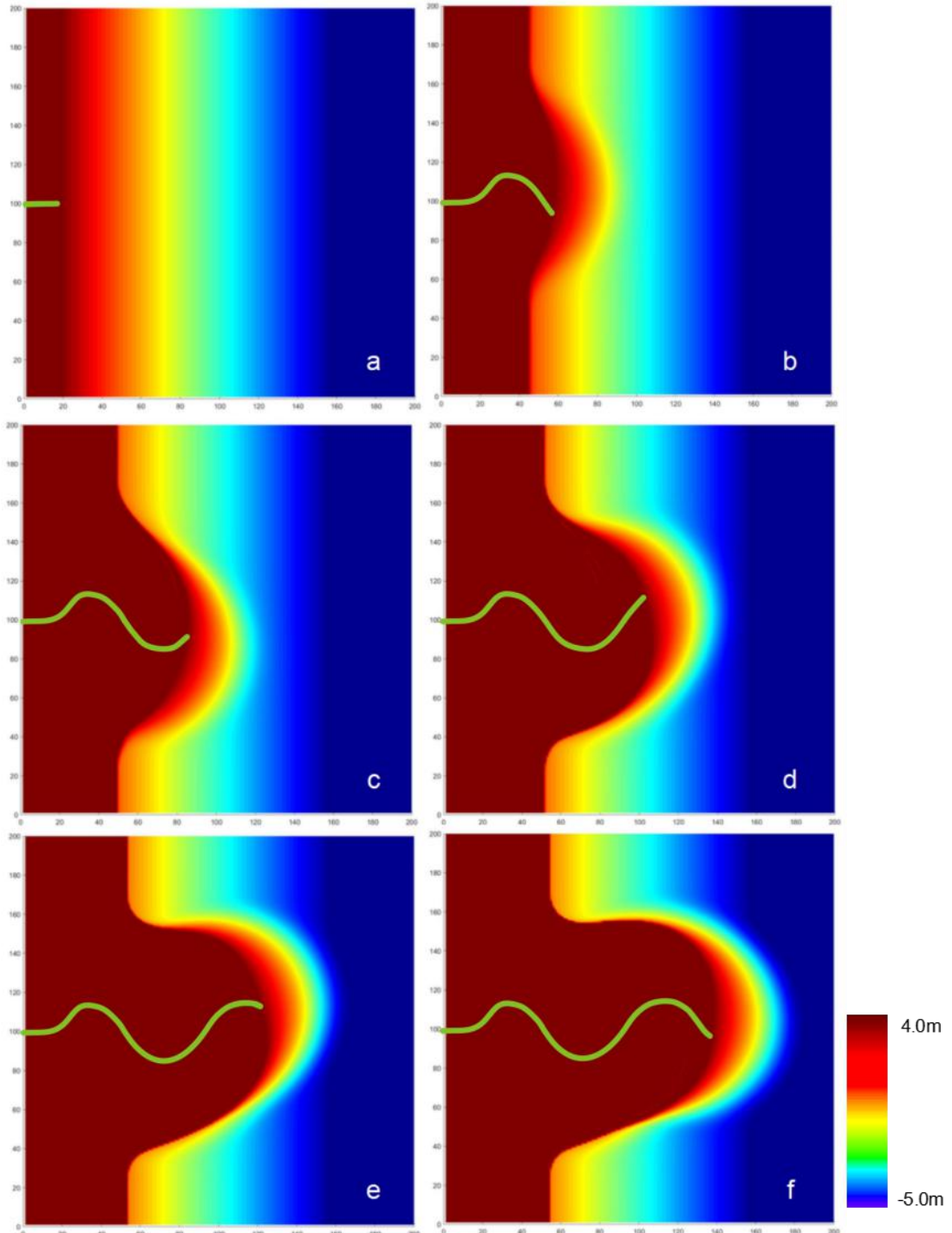


Fig. 6 The initial topography and the simulated results of Model 1. (a): the initial topography; (b): the topography at $t=10$ Myr.



430

Fig. 7 Plane view of Model 1 results. (a): $t=0$ Myr; (b): $t=2$ Myr; (c): $t=4$ Myr; (d): $t=6$ Myr; (e): $t=8$ Myr; (f): $t=10$ Myr.

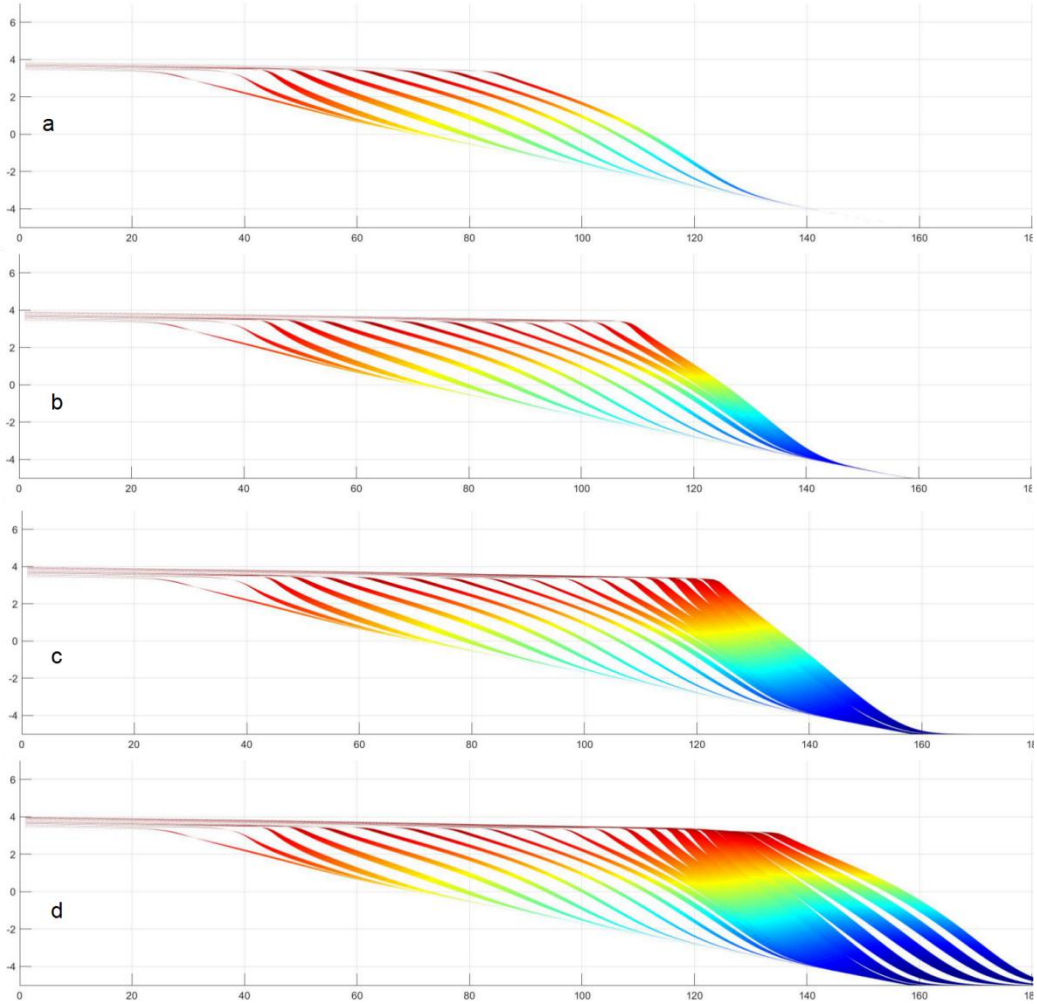


Fig. 8 Cross section at $x=75\text{m}$. (a): $t=4\text{Myr}$; (b): $t=6\text{ Myr}$; (c): $t=8\text{Myr}$; (d) $t=10\text{Myr}$. The blank spaces divide the strata into isochronous stratigraphic units, which can be used to infer the relative deposition rate.

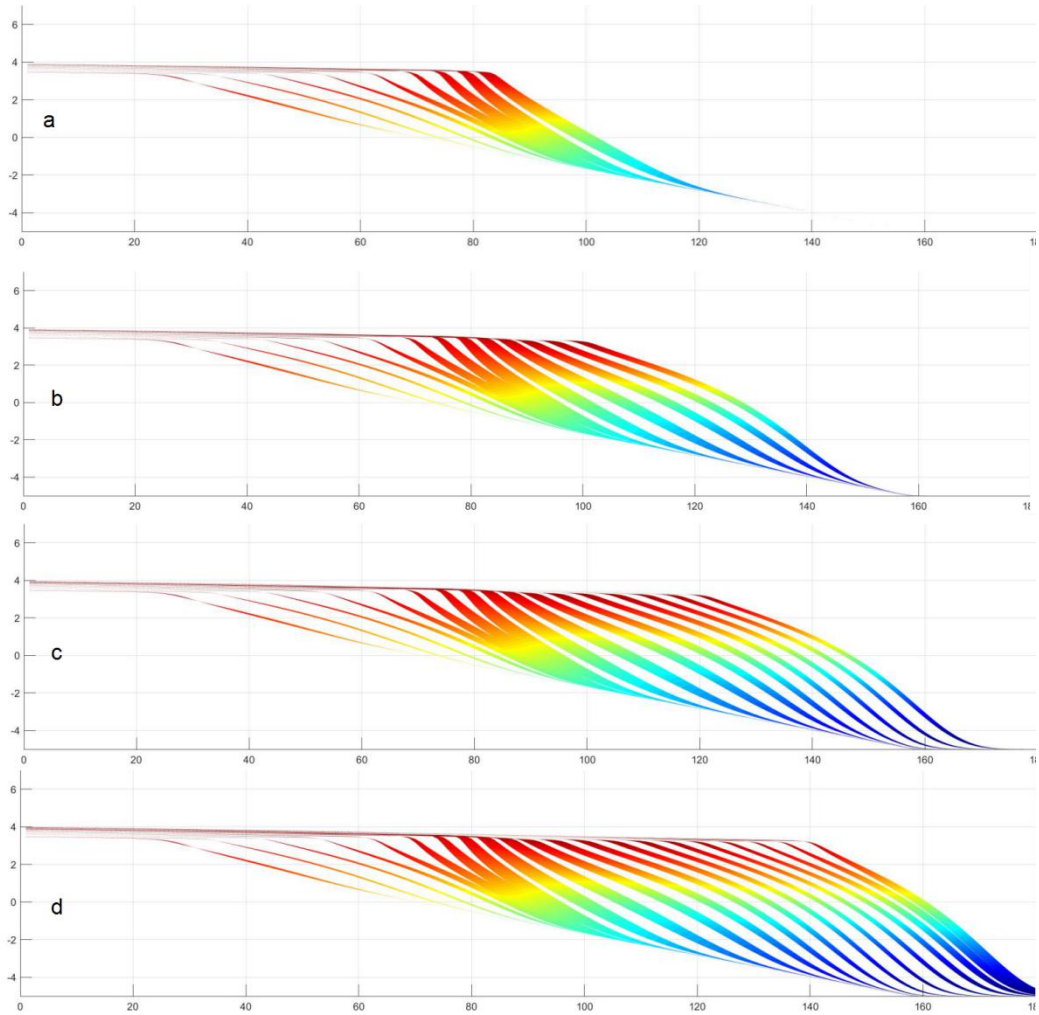


Fig. 9 Cross section at $x=125\text{m}$. (a): $t=4\text{Myr}$; (b): $t=6\text{ Myr}$; (c): $t=8\text{Myr}$; (d): $t=10\text{Myr}$. The blank spaces divide the strata into isochronous stratigraphic units, which can be used to infer the relative deposition rate.

440

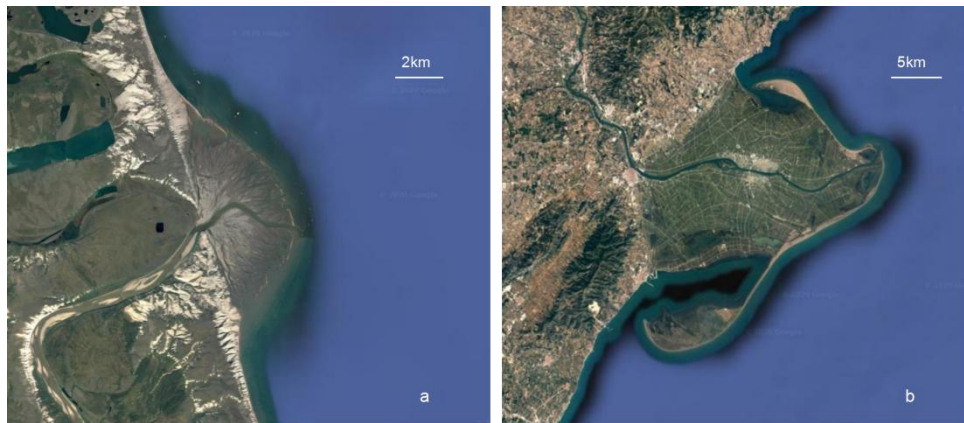


Fig. 10 Horton River Delta in Canada (a) and Ebro Delta in Mediterranean Sea (b) (taken from © Google Maps)

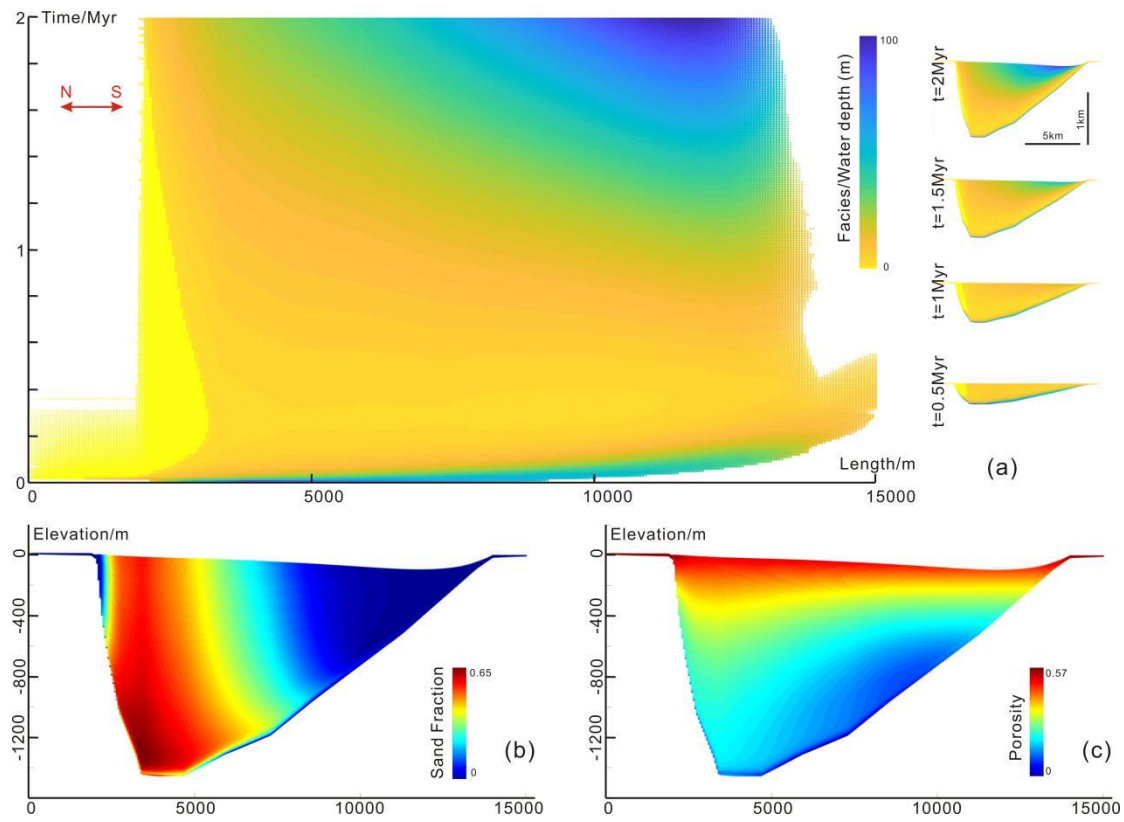
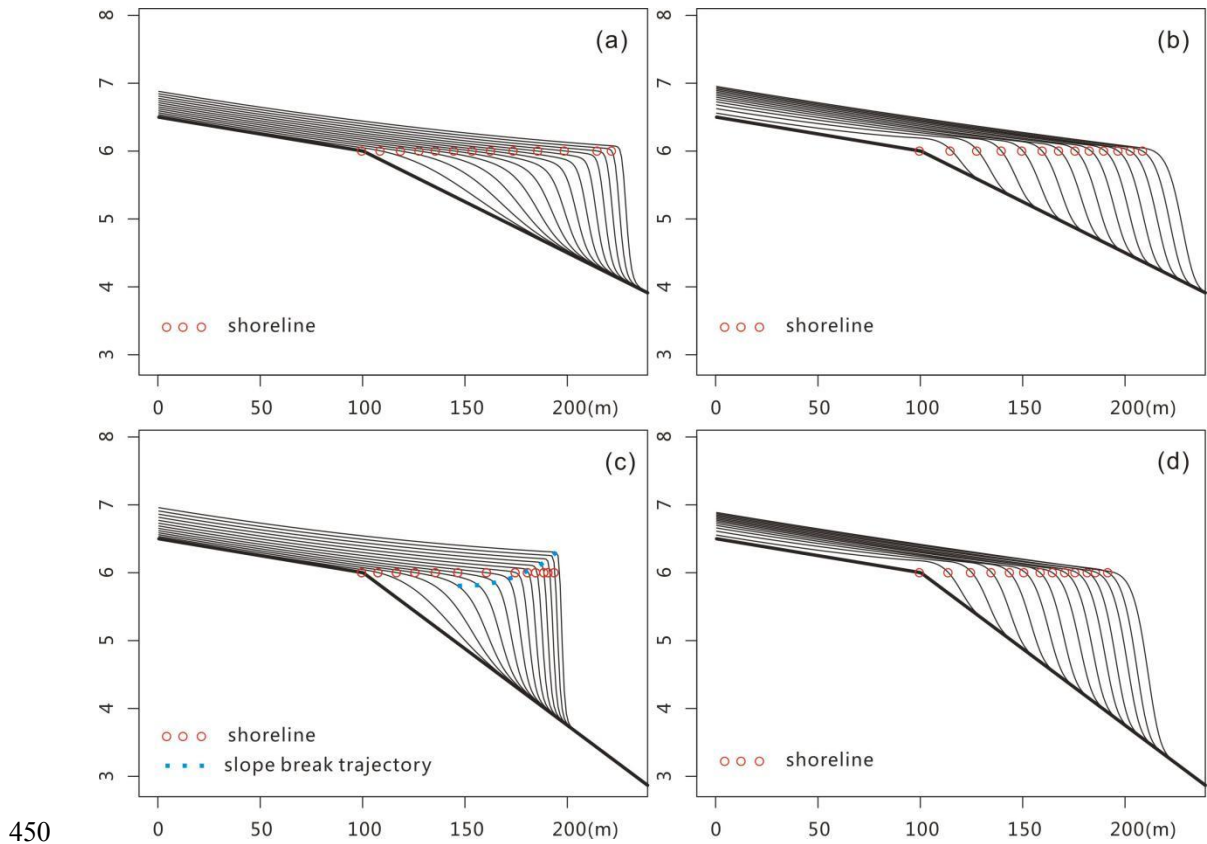


Fig. 11 Simulation results of Gaobei Slope Belt during the study interval. a) Sedapp results of facies in the time domain (Wheeler diagram) and depth domain at different times; b) Sedapp results of sand fraction in the depth domain. c) Sedapp results of porosity in the depth domain



450 Fig. 12 Comparison of the simulated results by water-depth based algorithm and the algorithm of Sedapp. a) Cliniforms of gentle slope created in water depth models; b) Cliniforms of gentle slope created in Sedapp; a) Cliniforms of steep slope created in water depth models; d) Cliniforms of steep slope created in Sedapp. The results of the two algorithms did not diverge strongly when the original slope was gentle, while the cliniform shapes and slope break trajectories could be very different when 455 the slope was steep.

Tab. 1 Main simulation parameters of Model1 (see 2.1 above for meanings of the notations)

Parameter	Value
α	1000
β	500
η	2
α_{wd}	10000
β_{wd}	0.16
η_{wd}	1
ε	0
<i>Der</i>	1